

Variability and spectral energy distributions of low-luminosity active galactic nuclei: a simultaneous X-ray/UV look with *Swift*

E. Pian,^{1,2,3*} P. Romano,⁴ D. Maoz,⁵ A. Cucchiara,⁶ C. Pagani⁶ and V. La Parola⁴

¹INAF, Osservatorio Astronomico di Trieste, Via G. Tiepolo 11, I-34143 Trieste, Italy

²Scuola Normale Superiore, Piazza dei Cavalieri 7, I-56126 Pisa, Italy

³European Southern Observatory, Karl-Schwarzschild-Strasse 2, D-85748 Garching bei München, Germany

⁴INAF, Istituto di Astrofisica Spaziale e Fisica Cosmica, Via U. La Malfa 153, I-90146 Palermo, Italy

⁵School of Physics and Astronomy, Tel-Aviv University, Tel-Aviv 69978, Israel

⁶Department of Astronomy and Astrophysics, Pennsylvania State University, 525 Davey Laboratory, University Park, PA 16802, USA

Accepted 2009 September 9. Received 2009 September 9; in original form 2009 July 27

ABSTRACT

We have observed four low-luminosity active galactic nuclei (AGNs) classified as type 1 Low-Ionization Nuclear Emission-Line Regions (LINERs) with the X-Ray Telescope (XRT) and the Ultraviolet–Optical Telescope (UVOT) onboard *Swift*, in an attempt to clarify the main powering mechanism of this class of nearby sources. Among our targets, we detect X-ray variability in NGC 3998 for the first time. The light curves of this object reveal variations of up to 30 per cent amplitude in half a day, with no significant spectral variability on this time-scale. We also observe a decrease of ~ 30 per cent over 9 d, with significant spectral softening. Moreover, the X-ray flux is ~ 40 per cent lower than observed in previous years. Variability is detected in M81 as well, at levels comparable to those reported previously: a flux increase in the hard X-rays (1–10 keV) of 30 per cent in ~ 3 h and variations by up to a factor of 2 within a few years. This X-ray behaviour is similar to that of higher luminosity, Seyfert-type objects. Using previous high-angular-resolution imaging data from the *Hubble Space Telescope* (*HST*), we evaluate the diffuse UV emission due to the host galaxy and isolate the nuclear flux in our UVOT observations. All sources are detected in the UV band, at levels similar to those of the previous observations with *HST*. The XRT (0.2–10 keV) spectra are well described by single power laws and the UV-to-X-ray flux ratios are again consistent with those of Seyferts and radio-loud AGNs of higher luminosity. The similarity in X-ray variability and broad-band energy distributions suggests the presence of similar accretion and radiation processes in low- and high-luminosity AGNs.

Key words: galaxies: active – galaxies: nuclei – ultraviolet: galaxies – X-rays: galaxies.

1 INTRODUCTION

Low-luminosity active galactic nuclei (AGNs) are a common phenomenon, with a large fraction of all massive galaxies displaying some weak activity that is likely of non-stellar origin (see e.g. Ho 2008, and references therein). Understanding the demographics and physics of these objects is a necessary step towards the comprehension of supermassive black hole activity in the local Universe and its past evolution. Low-Ionization Nuclear Emission-Line Regions (LINERs), in particular, are a class of low-luminosity AGNs defined on the basis of their optical spectral line ratios (Heckman 1980; Ho 2008) and can be further divided into various sub-

classes according to their different properties (Chiaberge, Capetti & Macchetto 2005; Gonzalez-Martin et al. 2009). A fundamental question about these sources is the origin of their optical spectrum and multiwavelength emission in general: it is not clear which fraction of the powering source is non-stellar and, if it is due to accretion, what is the regime of the accretion and the efficiency of the radiation conversion. It has been argued that the lack of X-ray variability (e.g. Komossa, Böhringer & Huchra 1999; Roberts, Warwick & Ohashi 1999; Georgantopoulos et al. 2002; Pellegrini et al. 2003; Ho 2008), the non-detection of broad Fe $K\alpha$ lines down to stringent limits (Ptak et al. 2004) and the weakness or absence of the characteristic ‘big blue bump’ in their optical/near-ultraviolet (UV) spectra, traditionally observed in Seyferts (Quataert et al. 1999; Chiaberge et al. 2006), indicate that their engines may be intrinsically different from those of the more luminous AGNs, and could consist of radiatively inefficient accretion flows (RIAFs).

*E-mail: elena.pian@sns.it

Table 1. Target parameters.

Name	Distance (Mpc)	N_{H}^{Ga} (10^{20} cm^{-2})	N_{H}^{b} (10^{20} cm^{-2})	Γ^{c}	$\chi^2_{\text{red}}/\text{d.o.f.}$	F^{d} (0.2–1 keV)	F^{d} (1–10 keV)	L_{UV}^{e}	$L/L_{\text{Edd}}^{\text{f}}$
M81	3.6	5.55	$10.45^{+0.93}_{-0.89}$	2.04 ± 0.04	0.966/290	11.2 ± 0.1	14.9 ± 0.4	1.4	8.8×10^{-6}
NGC 3998	13.1	1.01	$6.85^{+1.26}_{-1.20}$	1.95 ± 0.06	0.948/188	$6.2^{+0.1}_{-0.8}$	$9.8^{+0.5}_{-0.4}$	6.0	1.1×10^{-5}
NGC 4203	15.1	1.11	$2.74^{+4.51}_{-2.74}$	$1.81^{+0.24}_{-0.21}$	0.699/16	$1.4^{+0.2}_{-0.4}$	$2.8^{+0.6}_{-0.4}$	4.0	1.1×10^{-4}
NGC 4579	21	2.97	$7.01^{+1.43}_{-1.34}$	1.92 ± 0.07	0.972/145	4.1 ± 0.1	6.8 ± 0.4	9.8	7.4×10^{-5}

^aHydrogen column densities derived from Kalberla et al. (2005) and consistent with the A_B extinction values reported in (Maoz 2007), using a typical Milky Way gas-to-dust ratio, $5 \times 10^{21} \text{ cm}^{-2} \text{ mag}^{-1}$.

^bHydrogen column densities from the XRT spectral fits.

^cPhoton index, $f_E \propto E^{-\Gamma}$.

^dUnabsorbed flux in units of $10^{-12} \text{ erg cm}^{-2} \text{ s}^{-1}$.

^eUnabsorbed monochromatic luminosity at 2500 Å, in units of $10^{25} \text{ erg s}^{-1} \text{ Hz}^{-1}$.

^fEddington ratio based on the observed SEDs.

However, X-ray observations of most of these sources have been sparse and not sensitive or not long enough to detect significant variability, except in M81, one of the closest and best studied *bona fide* (e.g. Kewley et al. 2006) LINERs. Furthermore, UV monitoring with the *Hubble Space Telescope* (*HST*) Advanced Camera for Surveys (ACS) of a sample of 17 LINERs has revealed the presence of bright and variable UV nuclei (Maoz et al. 2005). By coupling these UV measurements with non-simultaneous X-ray measurements with *ASCA*, *Chandra* and *XMM-Newton*, Maoz (2007) has shown that the UV-to-X-ray flux ratios in LINERs are similar to those of much-more-luminous Seyferts. Thus, contrary to the common paradigm, rather than being qualitatively different from Seyferts, LINERs may instead be ‘scaled-down’ analogues of Seyferts, with similar emission mechanisms operating in both classes.

While the arguments of Maoz (2007) are supported by accurate photometry, the UV and X-ray data of his sample were not simultaneous, with measurements often separated by years. LINERs exhibit variability, which, albeit not of very large amplitude (by factors of up to a few in the UV on time-scales of years; Maoz et al. 2005), may undermine the results derived from non-simultaneous observations. In this paper, we approach this problem by obtaining, for the first time, simultaneous X-ray and UV data, along with X-ray variability information, for a small sample of LINERs. The NASA satellite *Swift* is well suited to this task because it is a flexible and efficient facility for long simultaneous and accurate UV and X-ray monitoring. Results of this work have been presented in preliminary form in Romano et al. (2009).

Throughout this paper the uncertainties are given at 90 per cent confidence levels for one interesting parameter (i.e. $\Delta\chi^2 = 2.71$), unless otherwise stated. The spectral indices are parametrized as $F_\nu \propto \nu^{-\alpha}$, where F_ν ($\text{erg cm}^{-2} \text{ s}^{-1} \text{ Hz}^{-1}$) is the flux density as a function of frequency ν ; we also use $\Gamma = \alpha + 1$ as the photon index, $N(E) \propto E^{-\Gamma}$ (photon $\text{cm}^{-2} \text{ s}^{-1} \text{ keV}^{-1}$). This paper is organized as follows. In Section 2 we describe our sample, observations, analysis and results obtained with the two *Swift* instruments; in Section 3 we construct the spectral energy distributions (SED) and in Section 4 we discuss our findings.

2 SAMPLE, OBSERVATIONS, DATA ANALYSIS AND RESULTS

Our sample consists of the brightest LINERs in the Maoz (2007) UV sample, but excluding M87, because of its prominent jet, which would dominate the UV emission at the *Swift* resolution. The sample

includes M81, NGC 3998, NGC 4203 and NGC 4579 (see Table 1), which are all type 1 LINERs (i.e. with detected broad H α components) according to the classification by Ho et al. (1997). These four objects form a rather homogeneous sample (see Maoz 2007): all have similar UV and X-ray luminosities (10^{40} to $10^{41} \text{ erg s}^{-1}$), radio loudness parameters (~ 100), optical-to-X-ray indices $\alpha_{\text{ox}} (\sim 1)$, central black hole masses (10^7 to $10^{8.4} M_\odot$, three of which are measured directly from stellar or gas kinematics) and Eddington ratios (-4.5 to -5.5).

The *Swift* archive¹ already contained data for two of these sources, M81 and NGC 4203, which had been observed as *Swift* fill-in targets, and which we retrieved. M81 was observed for 33.7 ks and has an X-Ray Telescope (XRT; Burrows et al. 2005) spectrum of excellent quality. NGC 4203 had a good XRT spectrum, although somewhat underexposed compared to M81 (5.3 ks). We observed NGC 3998 and NGC 4579 with *Swift* for the first time as Targets of Opportunity (ToO) for 27.4 and 20.8 ks, respectively.

2.1 XRT

Table 2 reports the log of the *Swift*/XRT observations used for this work. The XRT data were processed with standard procedures (XRTPIPELINE v0.11.6), filtering and screening criteria by using FTOOLS in the HEASOFT package (v.6.4). Given the low count rate of the sources during the respective observing campaigns ($< 0.5 \text{ counts s}^{-1}$), we only considered photon counting data (PC), and further selected XRT grades 0–12. No pile-up correction was required. The source events were extracted in circular regions centred on the source, with radii depending on the source intensity (10–20 pixels, 1 pixel ~ 2.37 arcsec), while background events were extracted in source-free annular or circular regions, depending on the field.

Spectra were extracted for each XRT observation, as well as for the cumulative observing campaigns. Ancillary response files were generated with XRTMKARF, and account for different extraction regions, vignetting and point spread function (PSF) corrections. We used the v010 spectral redistribution matrices available in the calibration data base maintained by HEASARC. All spectra were rebinned with a minimum of 20 counts per energy bin to allow χ^2 fitting within XSPEC (v11.3.2).

We extracted XRT light curves from the same regions as for the spectra for source and background in the standard bands, 0.2–10 keV (total), 0.2–1 keV (soft, S) and 1–10 keV (hard, H). For our

¹ <http://swift.gsfc.nasa.gov/docs/swift/archive/>

Table 2. XRT observation log.

Name	Sequence ^a	Start time (UT) (yyyy-mm-dd hh:mm:ss)	End time (UT) (yyyy-mm-dd hh:mm:ss)	Exposure (s)
M81	00035059001	2005-04-21 00:47:46	2005-04-21 23:11:33	1 563
	00035059002	2005-08-25 01:20:04	2005-08-25 23:59:59	5 022
	00035059003	2006-06-24 00:05:06	2006-06-24 08:02:57	4 140
	00035059004	2006-11-18 01:05:11	2006-11-20 23:54:55	20 986
	00259527001	2007-02-06 21:44:17	2007-02-06 23:13:04	1 973
NGC 3998	00030916001	2007-04-20 15:03:58	2007-04-20 16:49:57	1 198
	00030916002	2007-04-29 02:39:06	2007-04-30 14:32:27	26 216
NGC 4203	00035477001	2005-12-25 00:05:03	2005-12-25 07:04:59	5 261
NGC 4579	00030939001	2007-05-15 00:56:39	2007-05-15 14:07:01	7 712
	00030939002	2007-05-16 01:08:52	2007-05-16 23:39:56	7 870
	00030939003	2007-05-17 01:18:44	2007-05-17 12:30:58	3 490
	00030939004	2007-05-18 10:53:03	2007-05-19 23:59:23	1 743

^aWe only considered data collected in PC observing mode.

analysis, we considered several time bins ranging from 120 s to the typical orbit duration ($\lesssim 5800$ s), and the minimum time bin was chosen to ensure that each light-curve point would have at least 30 source-plus-background counts. The exposure requirements were that the bins be at least 50 per cent exposed. In each case, the light curves were corrected for PSF losses, i.e. losses due to the extraction region geometry, and bad/hot pixels and columns falling within this region.

The host galaxy contribution in the XRT extraction region was evaluated using archival *Chandra* images of these LINERs obtained with the longest exposures with ACIS-S. We evaluated the counts in the following regions: (i) R1, an annulus with outer radius equal to the XRT extraction radius for each object and inner radius 4 arcsec, i.e. the radius including 99 per cent of the *Chandra* PSF; (ii) R2, a circular region of 4-arcsec radius; (iii) R3, an annular region of radii 4 and 4.5 arcsec. We assumed that R1 only contained host galaxy photons, R2 only active nucleus photons, while R3 was used to evaluate the galaxy counts in R2 assuming a constant host galaxy intensity profile. The measured counts in R3 were scaled to the area of R2 and added to the counts in R1, thus obtaining an estimate of the host galaxy counts in the whole XRT extraction region. The host galaxy contribution to the X-ray emission of the four LINERs ranges from 6 (NGC 3998) to 16 per cent (NGC 4203), and was therefore subsequently ignored.

M81 and NGC 3998 display a few very rapid (minute time-scale) flux changes of 30 to 60 per cent. Although this exceeds the typical level of XRT photometric stability, which is about 10 per cent (as established on the basis of the flux stability of the standard source PSR 0540–69; Cusumano, private communication), we note that these occur at low flux levels, so that we cannot assess their authenticity. Therefore, we have considered only fluxes integrated over time-scales no shorter than one orbit for further variability analysis.

Since the *Swift* satellite must resettles on the target at every orbit, the target’s location within the XRT field of view may change from orbit to orbit, and occasionally the source flux is greatly underestimated because of the vicinity of a detector dead column that affects the PSF to various degrees. We have systematically checked our observations for this effect and have corrected for it (see Grupe et al. 2007). However, because of the low flux level of our sources, in many cases the PSF reconstruction is not fully satisfactory and the corresponding flux points have been excluded from our variability analysis.

The orbit-averaged light curves of M81 and NGC 3998 indicate variability. In Figs 1(c), (d) and 2(b) we show the flux and hardness ratio time series of M81 and NGC 3998 during the pointings when significant variations were observed. The M81 hard X-ray light curves in 2006 June (Fig. 1c, middle panel) and November (Fig. 1d, middle panel) have $\chi^2 \simeq 30$ [for 5 degrees of freedom (d.o.f.)] and $\chi^2 \simeq 41$ (for 19 d.o.f.) with respect to the average flux, respectively, corresponding to probabilities of constancy of 10^{-3} or less. The variations in hard X-rays have a maximum amplitude of 30 per cent in a time-scale of 3 to 12 h. The variability in soft X-rays is less pronounced, but well correlated with the hard X-rays, so that the hardness ratio is not significantly variable on these time-scales. The soft and hard X-ray light curves of NGC 3998 on 2007 April 29 (Fig. 2b) are well correlated and have $\chi^2 \simeq 35$ (13 d.o.f.) and $\chi^2 \simeq 44$ (13 d.o.f.) with respect to the average flux, respectively, corresponding to constancy probabilities of 10^{-3} or less. The largest variability amplitude of NGC 3998 is about 30 per cent in both X-ray energy ranges, on a time-scale of about 12 h. Neither NGC 4203 (Fig. 3) nor NGC 4579 (Fig. 4) vary significantly in flux or hardness ratio on the orbit or longer time-scale.

We have evaluated the variability of M81 and NGC 3998 during the individual *Swift* pointings also through the excess variance parameter σ_{rms}^2 , defined as in Nandra et al. (1997) and Turner et al. (1999; see also Ptak et al. 1998). This never exceeds the value of 0.02 for both sources and for both energy ranges, and therefore it is almost one order of magnitude smaller than would be expected – based on the X-ray luminosities of these two LINERs – from the inverse proportionality relation between X-ray luminosity and variability established for Seyfert galaxies by Nandra et al. (1997) and Turner et al. (1999).²

For M81 and NGC 3998, which were observed on more than one epoch, with intervals larger than 1 d, we have evaluated the average flux at each epoch. The associated errors are the root mean squares of the averages, i.e. the standard deviations of the data points within the epoch, divided by the square root of their number. The corresponding light curves are shown in Figs 1(f) and 2(c) for M81 and NGC 3998, respectively. The long-term variations are conspicuous. The historical flux of M81 decreases between 2005 April and 2006

² Note that the durations of our XRT observations are similar to the monitoring times adopted by those authors, making the comparison of the σ_{rms}^2 parameters meaningful.

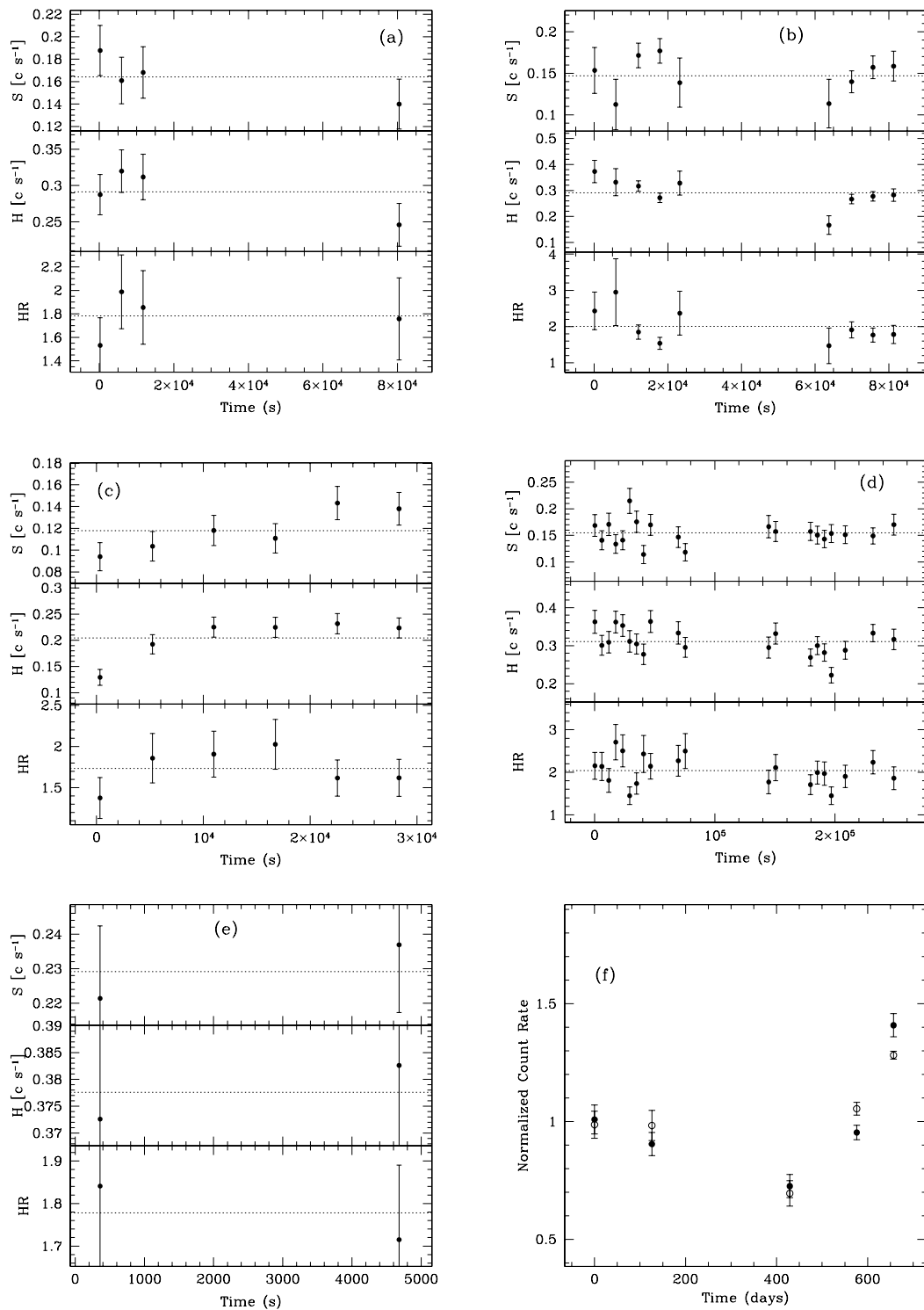


Figure 1. *Swift*/XRT background-subtracted light curves (count rate in counts s⁻¹) and hardness ratios (i.e. 1–10 to 0.2–1 keV flux ratios) of M81. The binning time interval corresponds to the orbit duration. Panels (a) to (e) report the 0.2–1 keV (top), 1–10 keV (middle) light curves and hardness ratio curves (bottom) of each pointing (see Table 2). Start times ($t = 0$) correspond to (a) 2005 April 21.033 UT, (b) 2005 August 25.056 UT, (c) 2006 June 24.004 UT, (d) 2006 November 18.045 UT, (e) 2007 February 6.906 UT. Panel (f) reports the 0.2–1 keV (filled circles) and 1–10 keV (open circles) light curves of M81 between 2005 and 2007. Each point is the average of the flux measured during each pointing in that given band and each curve is normalized to its average (0.16 and 0.29 counts s⁻¹ for the 0.2–1 and 1–10 keV curves, respectively). The time origin ($t = 0$) corresponds to 2005 April 21.0 UT.

June almost achromatically and then increases by 2007 February by a factor of 2 in the soft X-rays and slightly less in hard X-rays. The variability on year time-scales is well correlated in the two bands, with no significant variations of the hardness ratio. The 1–10 keV

flux of NGC 3998 decreases by 30 per cent in the 9 d separating our two observations, while the 0.2–1 keV flux decreases more slowly, implying a softening of the spectrum. Indeed, the hardness ratio (i.e. the 1–10 to 0.2–1 keV flux ratio) decreases significantly between

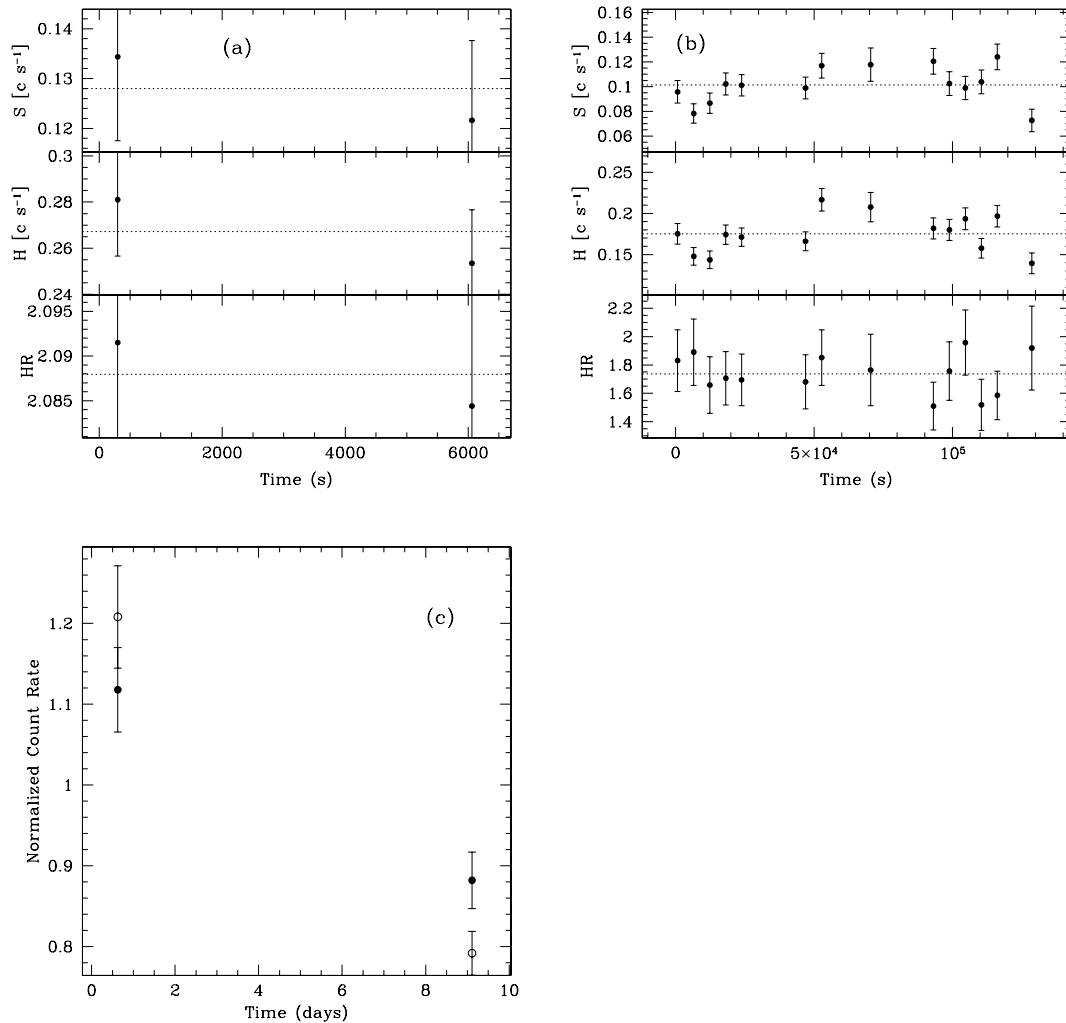


Figure 2. *Swift*/XRT background-subtracted light curves (count rate in counts s⁻¹) and hardness ratios (i.e. 1–10 to 0.2–1 keV flux ratios) of NGC 3998. The binning time interval corresponds to the orbit duration. Panels (a) and (b) report the 0.2–1 keV (top), 1–10 keV (middle) light curves and hardness ratio curves (bottom) of each pointing (see Table 2). Start times ($t = 0$) correspond to (a) 2007 April 20.628 UT, (b) 2007 April 29.11 UT. Panel (c) reports the 0.2–1 keV (filled circles) and 1–10 keV (open circles) light curves of NGC 3998 in 2007. Each point is the average of the flux measured during each pointing in that given band and each curve is normalized to its average (0.11 and 0.22 counts s⁻¹ for the 0.2–1 and 1–10 keV curves, respectively). The time origin ($t = 0$) corresponds to 2007 April 20.0 UT.

the two epochs, varying from $HR = 2.088 \pm 0.004$ to 1.75 ± 0.04 . However, a spectral fit with a single power law of each observation of this object does not show variability in the spectral parameters within the 90 per cent confidence level.

The mean XRT spectrum for each object was fit with a simple absorbed power-law model with free absorption and photon index. Fig. 5 shows the mean spectrum for each object in the sample, along with its best-fitting model, while the fit results are reported in Table 1. The spectra show no significant absorption features superimposed on the power-law continuum; however, M81 shows hints of a Fe K α emission line (6.4 keV, fixed), with an equivalent width $EW = 640^{+650}_{-410}$ eV. The F-test probability for this feature is 8.515×10^{-3} , which corresponds to a 2.6σ detection. NGC 4579 also shows a marginal (F-test probability of 3.207×10^{-2} or 2.1σ) Fe K α line at $6.4^{+0.2}_{-0.4}$ keV, with $EW = 550^{+5100}_{-310}$ eV. The fluxes of these lines are $(10^{+10}_{-4}) \times 10^{-14}$ and $(5^{+32}_{-2}) \times 10^{-14}$ erg cm⁻² s⁻¹, respectively. The equivalent widths are, within their large errors, broadly consistent with the values reported by Pellegrini et al. (2000a) and Terashima et al. (2002).

Although the uncertainties on the fitted hydrogen column densities (Table 1, column 4) are not small, all sources – except NGC 4203, whose spectrum has a poor signal-to-noise ratio – show significant evidence for absorption in excess of the Galactic one (also reported in Table 1).

2.2 UVOT

The *Swift* Ultraviolet–Optical Telescope (UVOT; Roming et al. 2005) observed the four targets with the filters *u* (3465 Å) *uvw1* (2600 Å), *uvw2* (2246 Å), *uvw2* (1928 Å) simultaneously with the XRT. The filter choice was driven by the objective of maximizing the nuclear signal, which is dominant in the UV, while minimizing the stellar emission from the bulge populations of the target galaxies. For each object, after verifying that the UVOT counts show no significant variability, we have co-added the images.

The data analysis was performed using the `UVOTSOURCE` task included in the latest `HEASOFT` software. This task normally calculates the magnitude by means of aperture photometry within a circular

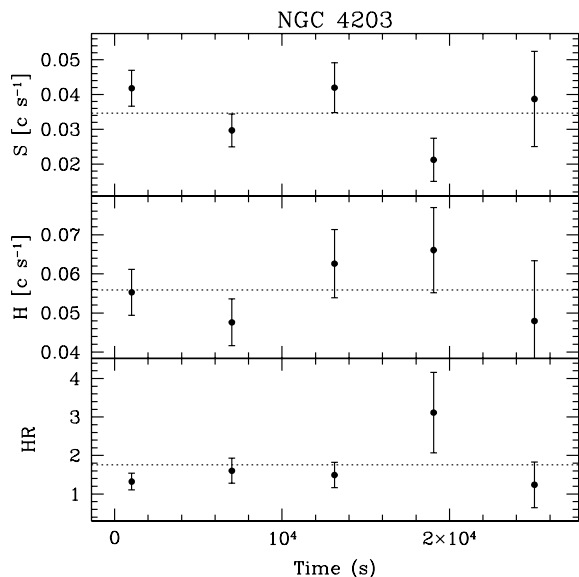


Figure 3. *Swift*/XRT background-subtracted light curves (count rate in counts s^{-1}) and hardness ratios (i.e. 1–10 to 0.2–1 keV flux ratios) of NGC 4203: 0.2–1 keV (top), 1–10 keV (middle) light curves and hardness ratio curves (bottom). The binning time interval corresponds to the orbit duration. The time origin ($t = 0$) corresponds to 2005 December 25.004 UT.

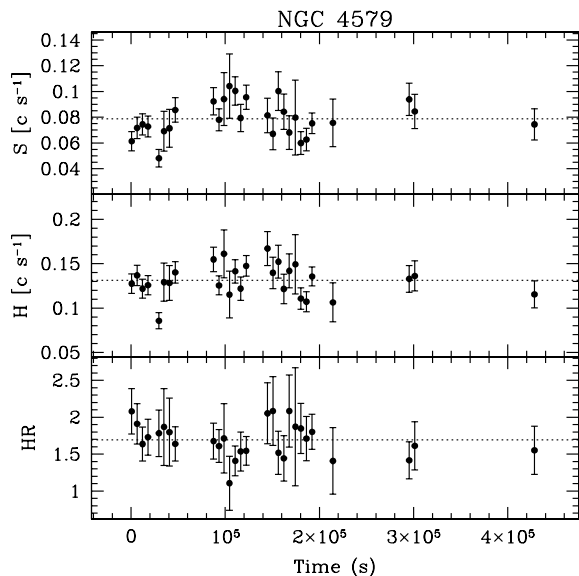


Figure 4. *Swift*/XRT background-subtracted light curves (count rate in counts s^{-1}) and hardness ratios (i.e. 1–10 to 0.2–1 keV flux ratios) of NGC 4579 during the four *Swift* pointings at this source: 0.2–1 keV (top), 1–10 keV (middle) light curves and hardness ratio curves (bottom). The binning time interval corresponds to the orbit duration. The time origin ($t = 0$) corresponds to 2007 May 15.039 UT.

region of 5-arcsec radius, which includes more than 99 per cent of the signal of a point source, and applies specific corrections due to the detector characteristics. Since the adoption of this standard aperture often resulted in oversubtraction of the host-galaxy background, we used instead an aperture of 2-arcsec radius, and applied the proper correction factor between a 2 and a 5 arcsec aperture (see below). Because of its proximity (3.6 Mpc), the host galaxy of M81 occupies most of the field-of-view of UVOT, making it difficult to estimate the sky background to be subtracted

from the nucleus and the galaxy light. The background was therefore computed from a 20.7 arcsec radius circular region separated by 6.5 arcmin from the nucleus. For uniformity, the remaining three LINERs, albeit more distant, were treated in the same way.

Using archival *HST* images of these LINERs at 2500 and 3300 Å obtained with the High Resolution Channel (HRC) of the *HST* ACS (Maoz et al. 2005), we have evaluated the nuclear point source subtracted host galaxy contribution for each object in a 2 arcsec radius circular area centred on the nucleus, and have interpolated or extrapolated the UV host galaxy fluxes to the central wavelengths of the UVOT u band and UV filters, in order to subtract them from the observed fluxes.

While the aperture-summed galaxy light is clearly detected in the *HST* images, the surface brightness is too low and the images are too oversampled to determine the surface brightness profiles of the galaxies on the scales of the apertures we use here. Different galaxy profiles will require different corrections for PSF losses outside the aperture. For the galaxy light subtraction, we have therefore considered two extreme cases: one in which the galaxy light is highly centrally concentrated, and one in which it has constant surface brightness. In the former scenario, the adoption of a 2-arcsec radius for the UVOT photometry results in a galaxy light loss similar to that suffered by the nuclear light, and therefore we first corrected the observed 2 arcsec radius flux to a 5 arcsec radius aperture, and then subtracted the galaxy flux evaluated from the *HST* images. In the latter case, where the light profile is flat, the galaxy light suffers no net PSF losses in the UVOT photometry, and we therefore first subtracted the *HST* galaxy flux from the total observed UVOT flux and then applied the 5 arcsec radius aperture correction to the remainder, which represents the point-source nuclear flux.

The host galaxy contribution is dominant in the u band (it is generally comparable to the total flux observed by UVOT) and decreases with decreasing wavelength to the $uvw2$ filter (1928 Å) where it contributes, at most, 50 per cent of the observed flux. The first galaxy-subtraction method described above predictably results in systematically larger nuclear fluxes than obtained with the second method. As also expected, the differences between the results of the two methods decrease as one goes to shorter wavelengths, where the galaxy light becomes less dominant.

All UVOT magnitudes have been converted into fluxes using the latest in-flight flux calibration factors and zero-points (Poole et al. 2008). The average observed fluxes with their statistical errors are reported in Table 3, where we also list the host galaxy fluxes measured in the *HST* images and converted to the wavelengths of the UVOT filters, and the final nuclear fluxes obtained with the two subtraction methods described above.

3 SED CONSTRUCTION

We combined the XRT spectra, corrected for the total hydrogen absorption (Table 1, column 4), and the UVOT fluxes, corrected for their host galaxy backgrounds and dereddened using the A_B extinction values compiled by Maoz (2007) from Schlegel, Finkbeiner & Davis (1998), and adopting the Galactic extinction curve of Cardelli, Clayton & Mathis (1989). These UV-to-X-ray spectral energy distributions (SED) are shown in Fig. 6. The errors associated with the UVOT nuclear fluxes are the sum in quadrature of the uncertainties associated with the observed UVOT fluxes (including the statistical error reported in Table 3 and the systematic errors given in Poole et al. 2008) and the uncertainties of the galaxy *HST* measurements (Table 3), increased by 5 per cent – summed in quadrature – to take into account the uncertainty in the background subtraction on the

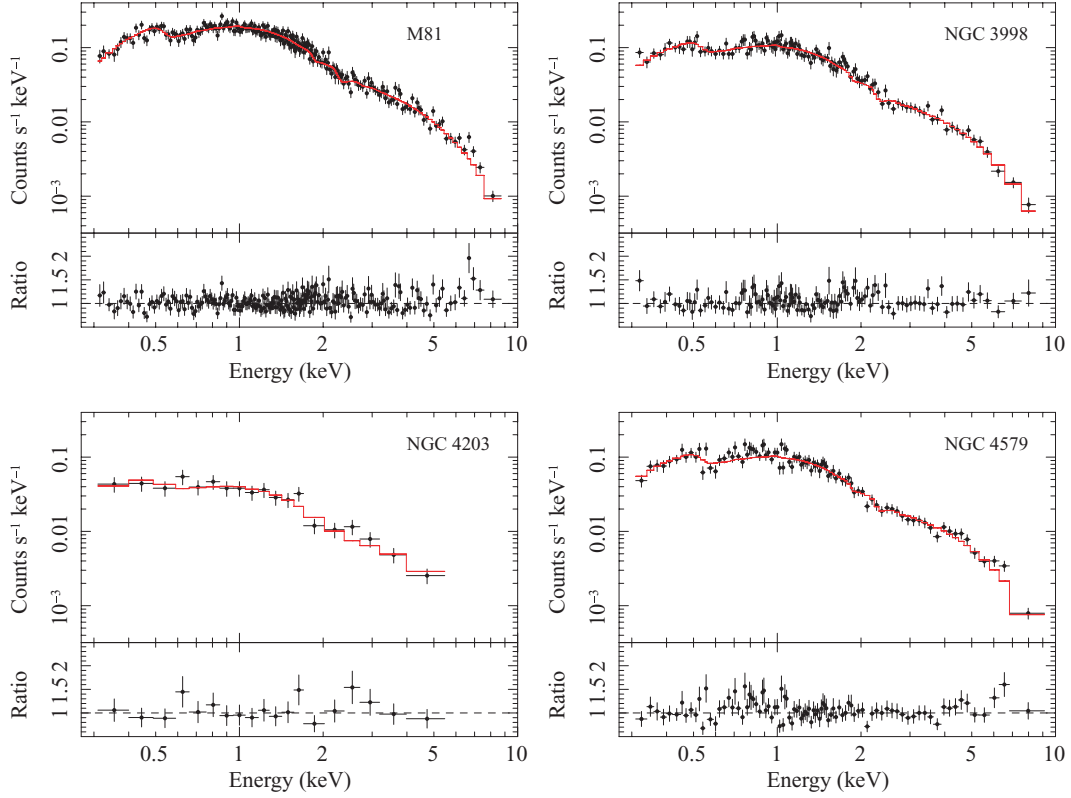


Figure 5. *Swift*/XRT spectra of the sample. The stepped curves represent the single absorbed power laws which best fit the spectra (see Table 1 for spectral parameters).

Table 3. *Swift*/UVOT observations.

Name	Band	Wavelength (Å)	Observed flux ^{a,b}	Galaxy flux ^{a,c}	Nuclear flux (1) ^{a,d,f}	Nuclear flux (2) ^{a,e,f}
M81	<i>u</i>	3465	5.40 ± 0.20	4.16 ± 0.03	1.2 ± 0.6	-6.3 ± 0.6
	<i>uvw1</i>	2600	4.50 ± 0.34	1.06 ± 0.03	3.4 ± 0.4	1.5 ± 0.4
	<i>uvm2</i>	2246	2.33 ± 0.25	0.53 ± 0.03	1.8 ± 0.4	0.9 ± 0.4
	<i>uvw2</i>	1928	3.39 ± 0.29	0.26 ± 0.03	3.1 ± 0.5	2.7 ± 0.5
NGC 3998	<i>u</i>	3465	5.73 ± 0.02	3.9 ± 0.1	1.8 ± 0.7	1.0 ± 0.7
	<i>uvw1</i>	2600	3.13 ± 0.01	2.4 ± 0.1	0.8 ± 0.3	0.3 ± 0.3
	<i>uvm2</i>	2246	2.46 ± 0.01	1.82 ± 0.03	0.6 ± 0.4	0.3 ± 0.4
	<i>uvw2</i>	1928	3.11 ± 0.01	1.39 ± 0.03	1.7 ± 0.4	1.4 ± 0.4
NGC 4203	<i>u</i>	3465	2.44 ± 0.07	2.35 ± 0.03	0.1 ± 0.3	-0.4 ± 0.3
	<i>uvw1</i>	2600	1.42 ± 0.04	0.56 ± 0.03	0.9 ± 0.1	0.8 ± 0.1
	<i>uvm2</i>	2246	0.62 ± 0.02	0.27 ± 0.03	0.3 ± 0.1	0.3 ± 0.1
	<i>uvw2</i>	1928	0.96 ± 0.04	0.13 ± 0.03	0.8 ± 0.1	0.8 ± 0.1
NGC 4579	<i>u</i>	3465	3.11 ± 0.06	2.74 ± 0.03	0.4 ± 0.3	-0.2 ± 0.3
	<i>uvw1</i>	2600	1.84 ± 0.03	1.33 ± 0.03	0.5 ± 0.1	0.3 ± 0.1
	<i>uvm2</i>	2246	1.55 ± 0.06	0.92 ± 0.03	0.6 ± 0.2	0.4 ± 0.2
	<i>uvw2</i>	1928	1.51 ± 0.03	0.62 ± 0.03	0.9 ± 0.2	0.8 ± 0.2

^aNot corrected for Galactic reddening, in 10^{-15} erg s $^{-1}$ cm $^{-2}$ Å $^{-1}$.

^bTotal flux, evaluated in a 2 arcsec radius circular area centred on the nucleus, and scaled to the equivalent flux in a 5 arcsec radius area using the UVOT PSF. The errors are statistical only (1σ).

^cExtranuclear galaxy flux within a 2 arcsec radius circular area centred on the nucleus, obtained by interpolating/extrapolating from archival *HST* ACS HRC images at 2500 and 3300 Å. The errors are statistical only (1σ).

^dNet nuclear flux, obtained by assuming that the host galaxy radial profile is highly centrally concentrated.

^eNet nuclear flux, obtained by assuming that the host galaxy radial profile is nearly flat, i.e. constant within the UVOT 2 arcsec radius aperture.

^fThe errors are propagated from the *Swift* UVOT and *HST* ACS HRC uncertainties and include the systematic uncertainties.

HST images and the interpolation/extrapolation errors. Whenever the galaxy flux evaluated from the *HST* images exceeded the total flux observed by UVOT, we have used the total uncertainty to compute a 3σ upper limit, which is indicated in the figure.

For comparison, we have plotted also the previously measured UV-to-X-ray measurements (see fig. 1 in Maoz 2007) and the mean SEDs of radio-loud and radio-quiet quasars from Elvis et al. (1994), normalized to go through the geometric mean of the two nuclear

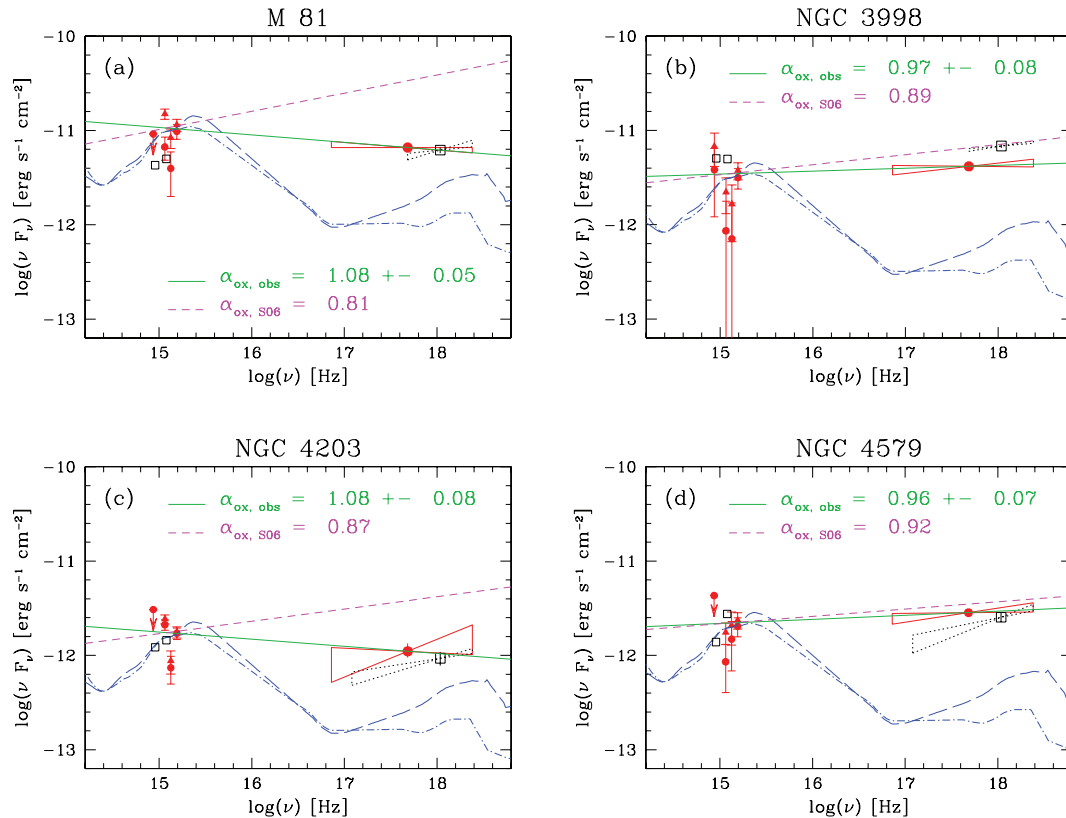


Figure 6. SEDs of our sample based on the simultaneous *Swift*/XRT and UVOT data from the present campaign (filled symbols) and from previous, non-simultaneous, *HST* UV and *Chandra*, *XMM-Newton* or *ASCA* X-ray observations (empty squares; Ho et al. 2001; Terashima et al. 2002; La Parola et al. 2004; Ptak et al. 2004; Maoz et al. 2005; Cappi et al. 2006; Maoz 2007). The optical–UV data, corrected for Galactic reddening, result from the observed UVOT fluxes, minus the *HST* host galaxy fluxes assuming that the host galaxy profile is strongly centrally concentrated (filled triangles) or constant with radius within the UVOT PSF (filled circles). When the latter method yields a negative flux (see Table 3), we replace both nuclear fluxes with a 3σ upper limit. The X-ray data are corrected for both Galactic and intrinsic absorption. The power laws fitting the XRT (solid bow-tie) and archival (dotted bow-tie) X-ray spectra are reported with their 90 per cent confidence boundaries. Similarly to Maoz (2007), we have superimposed on the data the mean spectra of radio-loud (long-dashed curve) and radio-quiet (dot-dashed curve) quasars from Elvis et al. (1994), and we have normalized them to the geometric mean of the 1928 Å nuclear fluxes obtained with the two methods of galaxy subtraction. We also show lines that connect the 2500 Å and 2 keV fluxes (solid) and the lines predicted by the S06 relation between α_{ox} and the monochromatic UV luminosities (short dash).

fluxes at 1928 Å obtained with the two galaxy subtraction methods described above. Note that the fluxes in this band suffer the least galaxy contamination, and therefore represent a solid lower limit to the intensity of the UV component.

4 DISCUSSION

We have observed four bright LINERs with XRT and UVOT onboard *Swift*, to study their variability and their simultaneous UV-to-X-ray ratios, in an attempt to probe their emission mechanisms. In particular, high-luminosity AGNs – Seyferts and quasi-stellar objects (QSOs) – are generally thought to be powered by geometrically thin and optically thick accretion discs. Our new data can bring new insight to the question of whether low-luminosity AGNs – specifically LINERs – are simply lower power analogues of Seyferts and QSOs, or are instead powered by some fundamentally distinct process, such as a RIAF.

Among our results is the first detection of X-ray variability in NGC 3998, in a range of time-scales from a few hours to days, with a ~ 30 per cent amplitude. This is in contrast to earlier reports of no X-ray variability during *BeppoSAX* and *XMM-Newton* observations (Pellegrini et al. 2000b; Ptak et al. 2004). The reason for this difference may be related to the larger sensitivity of XRT

with respect to *BeppoSAX*, and to XRT’s higher scheduling flexibility, which allows for longer monitoring periods than possible with *XMM-Newton*. Pellegrini et al. (2000b) have cited the absence of variability in NGC 3998 as evidence that the accretion is advection dominated in this source. Other workers (Ptak et al. 1998; Ho 2008) have, in general, invoked non-variability in X-rays as an indicator of a RIAF mode. Our finding of significant short-term X-ray flux variations in a low-luminosity LINER points, instead, to a similarity with whatever accretion mode is occurring in higher luminosity AGNs. However, the excess variance parameter of the NGC 3998 XRT light curves does not obey the inverse relation between X-ray luminosity and variability amplitude determined for high-luminosity AGNs (Nandra et al. 1997; Turner et al. 1999) when this is extrapolated to the X-ray luminosity of NGC 3998 (1.1×10^{40} erg s $^{-1}$ in 2–10 keV). Instead, the variability amplitude is similar to that typical of Seyferts of luminosity 10^{43} – 10^{44} erg s $^{-1}$ (2–10 keV). The range of validity of the relation may thus not extend to the low X-ray luminosities of the objects studied here.

A second LINER in our sample, M81, has already been shown to be X-ray variable on many time-scales, from hours to years (Pellegrini et al. 2000a; Iyomoto & Makishima 2001; La Parola et al. 2004; Page et al. 2004; Young et al. 2007; Markoff et al. 2008). Our findings confirm this behaviour and set this object,

along with NGC 3998, as another X-ray-variable low-luminosity AGN that is similar in this respect to high-luminosity AGNs. It has been suggested that the mechanisms active in this object are similar to those that cause the hard states in X-ray binaries (Markoff et al. 2008). Our observation of spectral softening accompanying source brightening on a time-scale of years is indeed reminiscent of the behaviour exhibited, on a shorter time-scale, by Galactic sources.

Our XRT timing results on NGC 4203 and NGC 4579 are inconclusive. NGC 4203 exhibits no significant X-ray variability on any time-scale, despite being, among the sources in Maoz (2007), the one that varied with the largest amplitude in the UV. One reason may be that our monitoring period was limited, and hence we did not catch the stochastically occurring variations. Alternatively, for this object the errors associated with orbit-averaged points are somewhat larger than those of M81 and NGC 3998, so that interorbit variations of amplitude similar to the interorbit variations in M81 and NGC 3998 would not be detected at high significance. A prominent, variable Fe $K\alpha$ emission line has been detected by *ASCA* and *XMM-Newton* in NGC 4579, and has given rise to various interpretations as to its origin from a standard accretion disc or a truncated disc (Terashima et al. 1998, 2000, 2002; Dewangan et al. 2004). Our weak XRT detection of the feature does not add significantly to this debate.

Our sources are all well detected in at least one UV filter (Fig. 6). The UV-to-X-ray SEDs compare rather well with those reported by Maoz (2007) and obtained with non-simultaneous UV and X-ray data. The X-ray spectrum of the LINERs always lies about a factor of 3 to 10 above the normalized radio-loud quasar template, depending on the object and on the wavelength. The UV flux level has not changed dramatically in any of the sources (Fig. 6), although these are among the most UV-variable sources in the Maoz (2007) sample. We note, however, that the UVOT fluxes are more uncertain than the *HST* measurements, owing to the galaxy subtraction and to the lower angular resolution and photometric accuracy of UVOT. The XRT fluxes and spectra are also similar to the older ones, except for NGC 3998, which XRT has detected in a state lower by ~ 40 per cent than observed in 1999 and 2001 by *BeppoSAX* and *XMM-Newton*, respectively (Ptak et al. 2004; see also Fig. 6b).

We have evaluated the Eddington ratios of our LINERs using the bolometric luminosities and the central black hole mass estimates compiled in Maoz (2007). The bolometric luminosities were obtained from the normalized templates of radio-loud AGNs (Elvis et al. 1994) from 3465 Å to 0.2 keV and the observed X-ray spectrum from 0.2 to 10 keV. In fact, the template may be a more reliable description of the spectrum at UV wavelengths (considering that some of our UV points are upper limits), while at X-rays the template always underestimates the real flux (see Fig. 6). In the radio-loud AGN spectrum, the UV-to-X-ray flux dominates the SED, representing more than half of the total emission. Moreover, considering that the *intrinsic* AGN spectra probably lack the conspicuous *observed* bump centred at 1 μm , due to reprocessed radiation at shorter wavelengths (Marconi et al. 2004), our computed bolometric luminosities may adequately represent the intrinsic luminosities after all. The Eddington ratios, reported in Table 1, are about 0.5 dex higher than those computed by Maoz (2007), who only included the UV luminosity, but are still low, as typical for LINERs.

By normalizing the AGN templates to the UV emission, we note that the precisely determined XRT spectral slopes follow the average radio-loud AGN shape, although, as noted, the spectral normalizations exceed the prediction by 0.5 to 1 order of magnitude (Fig. 6). Strateva et al. (2005) and Steffen et al. (2006, hereafter S06) have

studied the dependence of the optical-to-X-ray colour index, α_{ox} , of AGNs (defined – using our notation for the spectral indices, see last paragraph of Section 1 – as $\alpha_{\text{ox}} = -0.3838 \log(l_{2\text{keV}}/l_{2500\text{\AA}})$, where $l_{2\text{keV}}$ and $l_{2500\text{\AA}}$ are the rest-frame X-ray and UV monochromatic luminosities in $\text{erg s}^{-1} \text{Hz}^{-1}$, respectively) on the monochromatic rest-frame UV luminosity, and have found an empirical linear relation between those quantities (the parameters of the relation in the two works coincide, within the errors; we have used that of S06, which is based on a larger sample). We have extrapolated α_{ox} in the S06 relation, $\alpha_{\text{ox}} = 0.137 \log(l_{2500\text{\AA}}) - 2.638$ (note that we have changed the sign of their equation 2, to be coherent with our spectral index notation), by two orders of magnitude to low UV luminosities, corresponding to the observed monochromatic UV luminosities of the LINERs in our sample (extinction corrected, see Table 1, column 9). This extrapolation is plotted as a short-dashed line in Fig. 6. It can be compared to a power law passing through our *observed* luminosities at 2500 Å and 2 keV, shown in Fig. 6 as a solid line, with errors omitted, for clarity.

In NGC 3998 and NGC 4579 the observed values of α_{ox} coincide, to within the errors, with the extrapolation to low luminosities of the S06 relation. In M81 and NGC 4203, the less UV-luminous sources in our sample (see Table 1), $\alpha_{\text{ox,obs}}$ has an intermediate value, similar to those of Seyferts, and the extrapolated α_{ox} is significantly flatter than the observed one and predicts X-ray luminosities that are four–five times higher than observed. As already noted by S06 based on their data alone, and further pointed out by Maoz (2007) based on his non-simultaneous UV and X-ray measurements, the S06 relation probably flattens at luminosities below $\sim 10^{26} \text{ erg s}^{-1} \text{Hz}^{-1}$. Overall, our present simultaneous UV and X-ray photometry strengthens the case for a limiting value of α_{ox} below some critical luminosity typical of Seyferts.

In summary, for the LINERs under study, the significant UV emission, the X-ray intraday variability and the X-ray and multi-wavelength spectral similarity with radio-loud AGNs all point to continuity and similarity with AGNs of higher luminosity. In view of this, it is not clear that distinct accretion and radiation mechanisms are required in the different luminosity regimes. Further *Swift*/XRT and UVOT monitoring, or more optimally, new *HST* high angular resolution UV observations of larger samples, accompanied with XRT simultaneous coverage, could shed more light on these questions.

We note, finally, that we cannot exclude that, in these sources, the emission at X-ray and/or UV bands is partially due to a weak jet, some evidence of which has been reported for all of our four sources, either directly (for M81, based on resolved radio structure detection and radio polarization) or indirectly (for NGC 3998, NGC 4203, NGC 4579, based on a flat radio spectrum, a compact and variable radio core, and high brightness temperature) from high-resolution radio imaging (Bietenholz, Bartel & Rupen 2000, 2004; Bower, Falcke & Mellon 2002; Filho, Barthel & Ho 2002; Anderson, Ulvestad & Ho 2004; Ros & Perez Torres 2008). In the case of NGC 3998, a jet has been proposed by Ptak et al. (2004) as possibly responsible for the multiwavelength emission. Jetted high-energy radiation in this LINER would be compatible both with the rapid flux variations and with the frequency-dependent variability amplitude that we observe over 9 d (Fig. 2c), which is typical of non-thermal sources (e.g. Ulrich-H., Maraschi & Urry 1997), and which is dissimilar to the X-ray variability observed in Seyferts (usually of larger amplitude at softer energies e.g. Matsuoka et al. 1990; Nandra, Pounds & Stewart 1990; Edelson et al. 2000; Turner et al. 2001; Uttley & McHardy 2005; Terashima et al. 2009) and in weak-line radio galaxies (e.g. Gliozzi et al. 2008). However, it would be

premature to draw a conclusion on the exact nature of the X-ray emitting process from the detection of spectral softening accompanying flux decrease between only two epochs in this individual LINER. More work on the correlated radio and X-ray variability in LINERs – in both the observational and the theoretical directions – is necessary to assess the role of a jet in the multiwavelength emission (see e.g. Brenneman et al. 2009).

ACKNOWLEDGMENTS

We thank N. Gehrels for approving this set of ToOs and the *Swift* team, in particular the duty scientists and science planners, for making these observations possible. We are grateful to S. Immler and T. Belloni for kindly sharing their data on M81 and NGC 4203, G. Cusumano, D. Grupe, S. Holland and J. Nousek for advice on the *Swift* instruments and to C. Guidorzi for helpful discussion. We want to thank the anonymous referee for constructive comments that helped improving our presentation. PR thanks INAF-IASFMi, and DM thanks INAF – Osservatorio Astrofisico di Arcetri, where parts of this work were carried out, for their kind hospitality. This work was supported by grants ASI-INAF I/023/05/0 and ASI I/088/06/0. DM thanks the DFG for support via German–Israeli Project Cooperation grant STE1869/1-1.GE625/15-1. This research has made use of NASA’s Astrophysics Data System Bibliographic Services, as well as the NASA/IPAC Extragalactic Database (NED), which is operated by the Jet Propulsion Laboratory, California Institute of Technology, under contract with the National Aeronautics and Space Administration.

Facilities: *Chandra*, *Swift*, *Hubble Space Telescope*.

REFERENCES

- Anderson J. M., Ulvestad J. S., Ho L. C., 2004, *ApJ*, 603, 42
 Bietenholz M. F., Bartel N., Rupen M. P., 2000, *ApJ*, 532, 895
 Bietenholz M. F., Bartel N., Rupen M. P., 2004, *ApJ*, 615, 173
 Bower G. C., Falcke H., Mellon R. R., 2002, *ApJ*, 578, L103
 Brenneman L. et al., 2009, *ApJ*, 698, 528
 Burrows D. N. et al., 2005, *Space Sci. Rev.*, 120, 165
 Cappi M. et al., 2006, *A&A*, 446, 459
 Cardelli J. A., Clayton G. C., Mathis J. S., 1989, *ApJ*, 345, 245
 Chiaberge M., Capetti A., Macchetto F. D., 2005, *ApJ*, 625, 716
 Chiaberge M., Gilli R., Macchetto F. D., Sparks W. B., 2006, *ApJ*, 651, 728
 Dewangan G. C., Griffiths R. E., Di Matteo T., Schurch N. J., 2004, *ApJ*, 607, 788
 Edelson R. et al., 2000, *ApJ*, 534, 180
 Elvis M. et al., 1994, *ApJS*, 95, 1
 Filho M. E., Barthel P. D., Ho L. C., 2002, *A&A*, 385, 425
 Georgantopoulos I., Panessa F., Akylas A., Zezas A., Cappi M., Comastri A., 2002, *A&A*, 386, 60
 Gliozzi M., Foschini L., Sambruna R. M., Tavecchio F., 2008, *A&A*, 478, 723
 Gonzalez-Martin O., Masegosa J., Marquez I., Guainazzi M., Jimenez-Bailon E., 2009, *A&A*, in press (arXiv:0905.2973)
 Grupe D. et al., 2007, *ApJ*, 662, 443
 Heckman T. M., 1980, *A&A*, 87, 152
 Ho L. C., 2008, *ARA&A*, 46, 475
 Ho L. C., Filippenko A. V., Sargent W. L. W., 1997, *ApJS*, 112, 315
 Ho L. C. et al., 2001, *ApJ*, 549, L51
 Iyomoto N., Makishima K., 2001, *MNRAS*, 321, 767
 Kalberla P. M. W., Burton W. B., Hartmann D., Arnal E. M., Bajaja E., Morras R., Pöppel W. G. L., 2005, *A&A*, 440, 775
 Kewley L. J., Groves B., Kauffmann G., Heckman T. M., 2006, *MNRAS*, 372, 961
 Komossa S., Böhringer H., Huchra J. P., 1999, *A&A*, 349, 88
 La Parola V., Fabbiano G., Elvis M., Nicastro F., Kim D. W., Peres G., 2004, *ApJ*, 601, 831
 Maoz D., 2007, *MNRAS*, 377, 1696
 Maoz D., Nagar N. M., Falcke H., Wilson A. S., 2005, *ApJ*, 625, 699
 Marconi A., Risaliti G., Gilli R., Hunt L. K., Maiolino R., Salvati M., 2004, *MNRAS*, 351, 169
 Markoff S. et al., 2008, *ApJ*, 681, 905
 Matsuoka M., Piro L., Yamauchi M., Murakami T., 1990, *ApJ*, 361, 440
 Nandra K., Pounds K. A., Stewart G. C., 1990, *MNRAS*, 242, 660
 Nandra K., George I. M., Mushotzky R. F., Turner T. J., Yaqoob T., 1997, *ApJ*, 476, 70
 Page M. J., Soria R., Zane S., Wu K., Starling R. L. C., 2004, *A&A*, 422, 77
 Pellegrini S., Cappi M., Bassani L., Malaguti G., Palumbo G. G. C., Persic M., 2000a, *A&A*, 353, 447
 Pellegrini S., Cappi M., Bassani L., Della Ceca R., Palumbo G. G. C., 2000b, *A&A*, 360, 878
 Pellegrini S., Baldi A., Fabbiano G., Kim D.-W., 2003, *ApJ*, 597, 175
 Poole T. S. et al., 2008, *MNRAS*, 383, 627
 Ptak A., Yaqoob T., Mushotzky R., Serlemitsos P., Griffiths R., 1998, *ApJ*, 501, L37
 Ptak A., Terashima Y., Ho L. C., Quataert E., 2004, *ApJ*, 606, 173
 Quataert E., Di Matteo T., Narayan R., Ho L. C., 1999, *ApJ*, 525, L89
 Roberts T. P., Warwick R. S., Ohashi T., 1999, *MNRAS*, 304, 52
 Romano P., Pian E., Maoz D., Cucchiara A., Pagani C., La Parola V., 2009, in *Proc. 7th INTEGRAL Workshop*. SISSA, Trieste, p. 64 (arXiv:0905.1266)
 Roming P. W. A. et al., 2005, *Space Sci. Rev.*, 120, 95
 Ros E., Perez Torres M.-A., 2008, *Proceedings of Science*, *Proc. 9th European VLBI Network Symposium on the Role of VLBI in the Golden Age for Radio Astronomy and EVN Users Meeting*. SISSA, Trieste, p. 90 (arXiv:0811.4340)
 Schlegel D. J., Finkbeiner D. P., Davis M., 1998, *ApJ*, 500, 525
 Steffen A. T., Strateva I. V., Brandt W. N., Alexander D. M., Koekemoer A. M., Lehmer B. D., Schneider D. P., Vignali C., 2006, *AJ*, 131, 2826 (S06)
 Strateva I. V., Brandt W. N., Schneider D. P., Vanden Berk D. G., Vignali C., 2005, *AJ*, 130, 387
 Terashima Y., Kunieda H., Misaki K., Mushotzky R. F., Ptak A. F., Reichart G. A., 1998, *ApJ*, 503, 212
 Terashima Y., Ho L. C., Ptak A. F., Yaqoob T., Kunieda H., Misaki K., Serlemitsos P. J., 2000, *ApJ*, 535, L79
 Terashima Y., Iyomoto N., Ho L. C., Ptak A. F., 2002, *ApJS*, 139, 1
 Terashima Y. et al., 2009, *PASJ*, 61, 299
 Turner T. J., George I. M., Nandra K., Turcan D., 1999, *ApJ*, 524, 667
 Turner T. J., Romano P., George I. M., Edelson R., Collier S. J., Mathur S., Peterson B. M., 2001, *ApJ*, 561, 131
 Ulrich M.-H., Maraschi L., Urry C. M., 1997, *ARA&A*, 35, 445
 Uttley P., McHardy I. M., 2005, *MNRAS*, 363, 586
 Young A. J., Nowak M. A., Markoff S., Marshall H. L., Canizares C. R., 2007, *ApJ*, 669, 830

This paper has been typeset from a $\text{\TeX}/\text{\LaTeX}$ file prepared by the author.